Journal of Chemical, Biological and Physical Sciences

An International Peer Review E-3 Journal of Sciences

Available online at www.jcbsc.org

Section C: Physical Sciences

CODEN (USA): JCBPAT Research Article

Structural and Optical Properties of Zinc Doped Nickel Ferrite $Ni_{(1-x)}Zn_{(x)}Fe_2O_4$ Thin Films Prepared by Chemical Spray Pyrolysis Method

Nabeel A. Bakr*, Sabah A. Salman, Heyam F. Khudhair

Department of Physics, College of Science, University of Diyala, Diyala, IRAQ

Received: 14 December 2015; **Revised:** 06 January 2016; **Accepted:** 11 January 2016

Abstract: Nanocrystalline, homogeneous spinel $Ni_{(1-x)}Zn_{(x)}Fe_2O_4$ thin films (where x = 0, 0.02, 0.04, 0.06, 0.08 and 0.1) were deposited on glass substrates by using chemical spray pyrolysis (CSP) technique at substrate temperature of (400 ± 10) ^oC and thickness of about (300 ± 10) nm. Before characterization, all films were annealed in atmosphere ambient at temperature of 520 ^oC for 4 hours. The structural, morphological and optical properties of these films have been investigated using XRD, AFM, and UV-Visible spectroscopy respectively. The XRD results showed that all films are polycrystalline in nature with cubic structure and preferred orientation along (311) plane according to the (ICDD) card no. 10-0325. The crystallite size calculated by Scherrer's formula was found to be 14.18 nm for the undoped sample and decreases up to 3.94 nm for the sample with x = 0.10. It is observed also that the lattice constant of Ni–Zn ferrite thin films increases with growing concentration of Zn^{2+}, and this may be attributed to the smaller Ni^{2+} cations of smaller ionic radii (0.74 Å) being replaced by larger Zn^{2+} cations of larger ionic radii (0.84 Å). Moreover, the addition of Zn^{2+} ions causes the migration of Fe^{3+} ions from tetrahedral sites to octahedral sites. The AFM images show a uniform island-like topography and some structure of clusters could be clearly observed. The size of grains in clusters of the prepared thin films are in the range of several tens of nanometers, which is one order of magnitude higher than the crystallite size calculated from XRD patterns. The optical properties of these films have been studied using UV-Visible spectroscopy. The absorbance and transmittance spectra have been recorded in the wavelength range of

(300-900) nm in order to study the optical properties. The optical energy gap for allowed direct electronic transition was calculated using Tauc's equation and it is found to be 2.96 eV for the undoped Nickel Ferrite thin films. The optical constants including absorption coefficient (α), extinction coefficient (K_o), real and imaginary parts of dielectric constant were also calculated as a function of photon energy. In order to investigate the dispersion behavior of the refractive index of the prepared thin films, two terms of Cauchy's equation was applied to the n- λ data and the static refractive index (n_o) was calculated for all samples.

Keywords: Ni–Zn ferrite, Thin films, Spray pyrolysis, XRD, AFM, Optical properties

INTRODUCTION

Spinel ferrites with general formula AB_2O_4 are a large class of oxides with remarkable application possibilities from simple permanent magnets[1] to microwave applications[2], magnetic recording[3], gas sensors[4], catalysts[5] and photo-catalysts[6]. Generally, spinel ferrites have been applied for the last 70 years[7]. From all ferrites the Ni–Zn spinel ferrites are important as microwave materials, due to its high resistivity and low coercivity[1,7]. At the same time, Ni–Zn ferrites are structure sensitive and it is not easy to produce point-defect free, stoichiometric Ni–Zn ferrites for high resistivity applications. Since the miniaturization tendency of the electronic components started in the 1990s, the spinel ferrites have been prepared in the form of nano-structured thick and thin films. The properties of ferrite films depend on preparation route, due to their strong influence on type of the film (epitaxial or polycrystalline), microstructure, particle size, chemical homogeneity and cationic distribution between tetrahedral and octahedral sub-lattice sites[8]. For deposition of spinel ferrite polycrystalline thin films, different physical and chemical vapor deposition techniques are used[9–12].

The given methods are complicated, and expensive; and require special equipment and sometimes high processing temperatures above 500 °C[13]. As a low temperature method involving preparation of the ferrite film by using solution processing, sol–gel is combined with spin- or dip-coating[14]. However, sol–gel method usually requires many processing steps and expensive reagents, while commercial technology requires high quality and low cost ferrite films[7]. An alternative method to obtain spinel ferrite thin films is spray pyrolysis[15–17]. Generally, spray pyrolysis has been applied to deposit a wide variety of thin and thick metal oxide films since the 1970s[18]. Up to our knowledge, only few research papers can be found on Ni–Zn ferrites obtained by spray pyrolysis focusing on the investigation of structural and optical properties[15,16]. The aim of the present work is to deposit $Ni_{(1-x)}Zn_{(x)}Fe_2O_4$ thin films (where x = 0, 0.02, 0.04 , 0.06 , 0.08 and 0.1) on glass substrates by using spray pyrolysis and to investigate their structural, morphological and optical properties.

MATERIALS AND METHODS

Chemical spray pyrolysis technique was used to prepare Ni-$ZnFe_2O_4$ thin films on glass substrates using nickel nitrate hexahydrate $Ni(NO_3)_2.6H_2O$, zinc nitrate hexahydrate $Zn(NO_3)_2.6H_2O$ and iron nitrate nonahydrate $Fe(NO_3)_3.9H_2O$ as precursors sources. The glass substrates slides of (2.55 × 2.55 cm^2) dimensions, were cleaned by acetone solutions in an ultrasonic bath for (5) minutes and rinsed in distilled water and then dried by special fabric to get rid of any oil or dust and to ensure a clean surface which is necessary for the formation of nucleation center required for film deposition. Final solutions were prepared by mixing the starting solutions in appropriate volumetric proportions to get various

concentrations of Zn (0, 0.02, 0.04, 0.06, 0.08 and 0.1). The resultant solution was sprayed on glass substrate at temperature of (400 ± 10) ^{o}C. The thickness of the deposited films was about (300 ± 10) nm measured by the gravimetric method. Other deposition conditions were kept constant for each concentration as shown in **Table 1**. Before characterization, all films were annealed in atmosphere ambient at temperature of 520 ^{o}C for 4 hours.

Table 1: Experimental deposition conditions of sprayed $Ni_{(1-x)}Zn_{(x)}Fe_2O_4$ thin films

Nozzle-substrate distance	30 cm
Spray time	10 s
Spray interval	2 min.
Substrate temperature	400 °C
Pressure of the carrier gas	1.5 bar

The X-ray diffraction patterns for the prepared films were obtained in a (Shimadzu XRD-6000) goniometer using copper target (CuKα, 1.5418 Å). Atomic Force Microscopy (AFM) micrographs were recorded by using scanning probe microscope type (SPM- AA3000), contact mode, supplied by Angstrom Advanced Inc. Optical properties in the wavelength range of (300 - 900) nm were investigated by using UV-VIS-NIR spectroscopy (Shimadzu, UV-1800).

RESULTS AND DISCUSION

Structural analysis: X-ray diffraction studies were carried out on the deposited thin films to investigate the structural properties. **Figure 1** represents the XRD patterns of $Ni_{(1-x)}Zn_{(x)}Fe_2O_4$ (where x = 0, 0.02, 0.04, 0.06, 0.08 and 0.1). The XRD patterns show that the peaks at (2θ~ 30.2°, 35.6°, 43.3°, 57.3°, 62.9°) correspond to (220), (311), (400), (322), (422), (511) and (440) respectively which belong to the cubic spinel structure[19]. The peak corresponding to (311) plane at 2θ~35.6° is the most intense peak whereas other peaks are relatively low intense which is in agreement with the International Centre for Diffraction Data (ICDD) card number 10-0325. The crystallite size (D) for all films is calculated for (311) direction by Scherrer's formula[20]:

$$\mathbf{D}=\frac{\mathbf{K}\,\boldsymbol{\lambda}}{\boldsymbol{\beta}\cos\boldsymbol{\theta}} \qquad [1]$$

Where β is full width of half maximum, K is constant and was assumed to be equal to 0.9, λ is wavelength for Cu target for XRD instrument and θ is Bragg's angle. The crystallite size was found to be 14.18 nm for the undoped sample and decreases up to 3.94 nm for the sample with x = 0.10 as shown in **Figure 2**. The lattice constant (a_o) was also determined and the values are presented in **Table 2**. It can be seen from the values that the lattice constant increases with increasing zinc concentration x.

The observed increase in lattice constant of Ni–Zn ferrite thin films with growing concentration of Zn^{2+} is attributed to the smaller Ni^{2+} cations of smaller ionic radii (0.74 Å) being replaced by larger Zn^{2+}cations of larger ionic radii (0.84 Å). This result is in agreement with the results given by other reports[21,22]. Moreover, the addition of Zn^{2+} ions causes the migration of Fe^{3+} ions from tetrahedral sites to octahedral

sites. The Zn^{2+} ions being larger than Fe^{3+} ions expand the tetrahedral sites leading to an increase in the lattice parameter[23]. Overall, the obtained lattice constants of the prepared Ni–Zn ferrite thin films are smaller than the values obtained for Ni–Zn ferrite powders[24].

This could be attributed to the high values of micro stress induced in the films in comparison with the powders which are almost free of stress. An induced stress could appear in the films due to mismatch in the thermal expansion coefficients of the film and substrate[25,26].

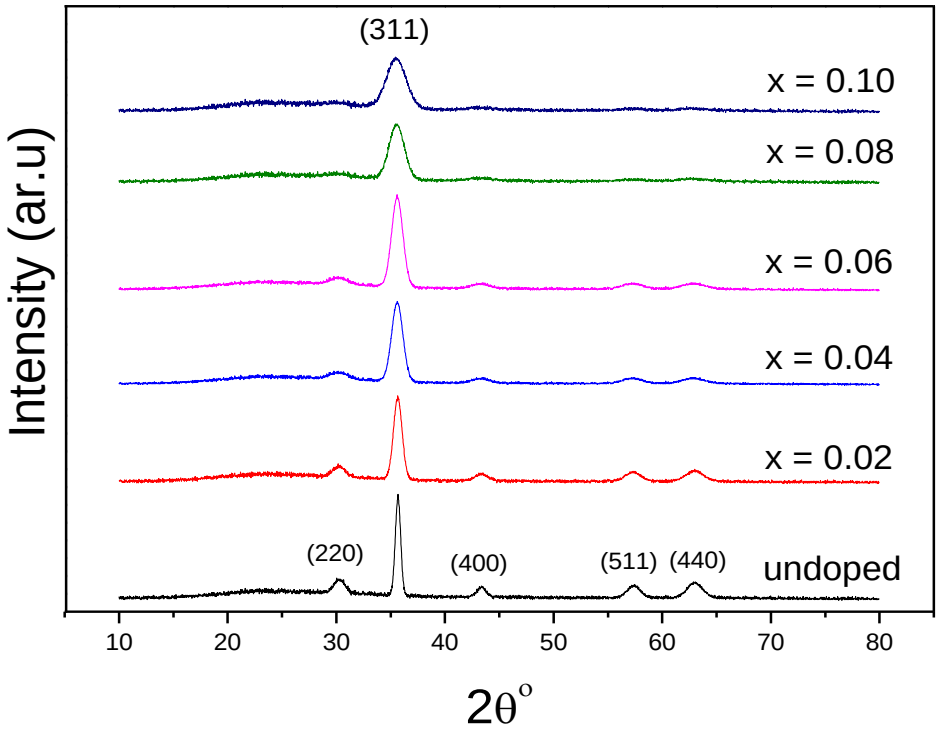

Figure 1: X-ray diffraction patterns of undoped $NiFe_2O_4$ and $Ni_{(1-x)}Zn_{(x)}Fe_2O_4$ thin films

Atomic Force Microscopy Analysis (AFM): The morphological investigation of $Ni_{(1-x)}Zn_{(x)}$ Fe_2O_4 (where x = 0, 0.02, 0.04, 0.06, 0.08 and 0.10) thin films deposited on glass substrates at (400 ± 10) ^oC was accomplished by using AFM. The size of the scanned area was (~ 2 × 2 μm^2). **Figure 3** shows the AFM images of $Ni_{(1-x)}Zn_{(x)}Fe_2O_4$ thin films.

The analysis of the AFM images shows homogenous and smooth thin films. The average grain size, average roughness and root mean square (RMS) roughness for all films, estimated from AFM, are given in **Table 3**. The undoped sample has the highest average grain size.

The images show uniform island-like topography and some structure of clusters can be clearly observed. These clusters are the result of crystallites coalescence[27]. The size of grains in clusters of $Ni_{(1-x)}Zn_{(x)}Fe_2O_4$ thin films are in the range of several tens of nanometers, which is one order of magnitude higher than the crystallite size calculated from XRD patterns.

Table 2: Structural parameters of $Ni_{(1-x)}Zn_{(x)}Fe_2O_4$ thin films

$Ni_{(1-x)}Zn_{(x)}Fe_2O_4$						
x	0	0.02	0.04	0.06	0.08	0.10
2Θ (deg)	35.6802	35.6602	35.6111	35.5905	35.5621	35.5214
hkl	311	311	311	311	311	311
d (Å)	2.514	2.516	2.519	2.519	2.522	2.525
FWHM (rad)	0.0102697	0.0164314	0.0213609	0.0242363	0.0287549	0.0369707
D (nm)	14.18	8.86	6.82	6.01	5.06	3.94
Lattice Constant (Å)	8.339	8.343	8.354	8.354	8.366	8.376

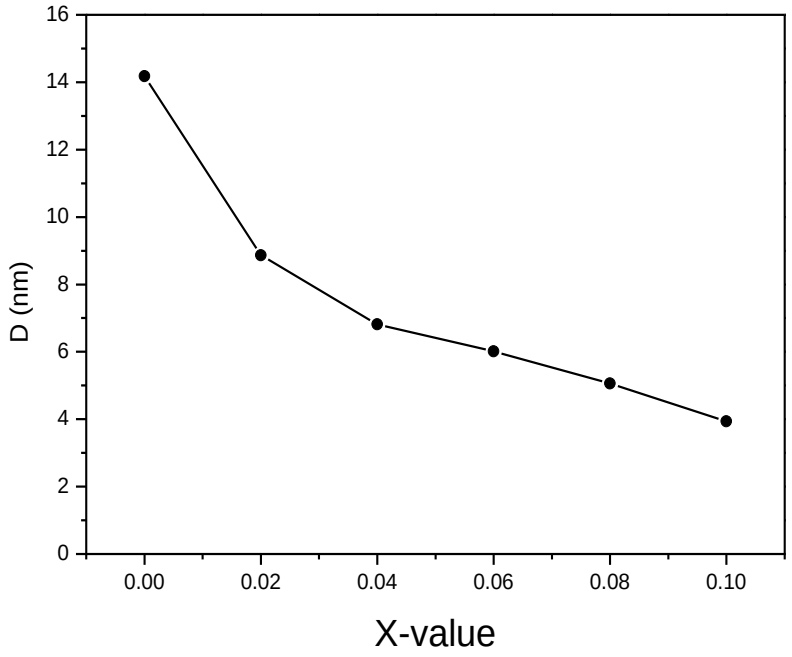

Figure 2: The crystallite size (D) of $Ni_{(1-x)}Zn_{(x)}Fe_2O_4$ thin films

Optical properties: Figure (4) shows the transmittance spectra in the range of (300 - 900) nm for Nickel-Zinc Ferrite thin films. The transmittance for all films increases as the wavelength increases in the range of (300 - 600) nm.

The spectra show high transparency in the visible and infrared regions, and low transparency in the ultraviolet region. It can also be observed that the fundamental absorption edge (which separates the high absorption region and the low absorption region or the window region) is not very sharp in the visible region of the spectrum.

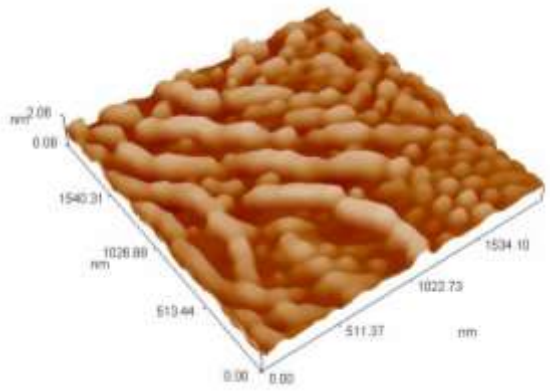

(undoped)

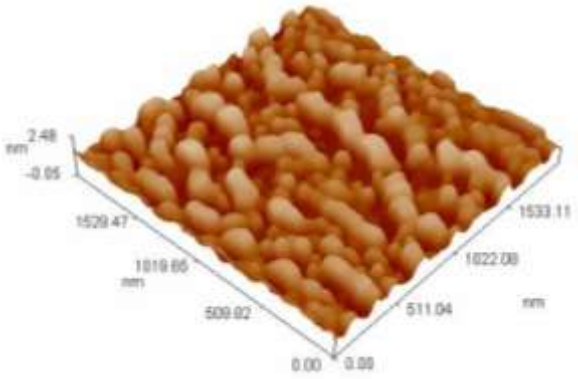

(x = 0.02)

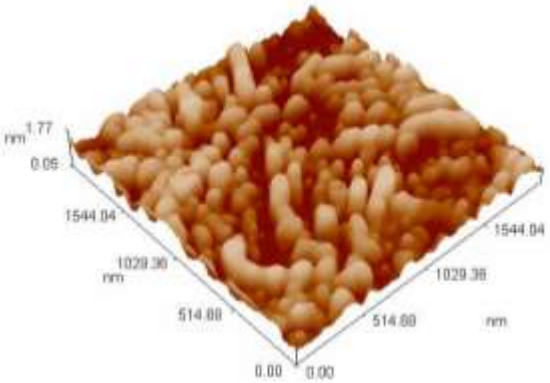

(x = 0.04)

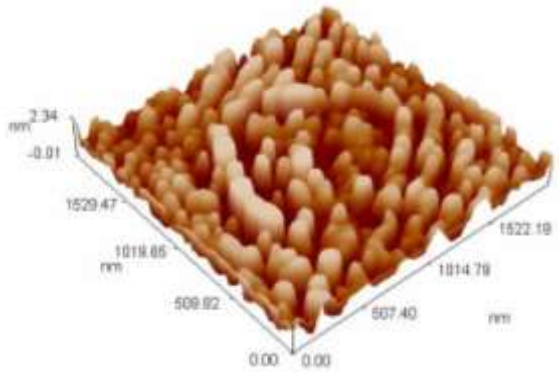

(x = 0.06)

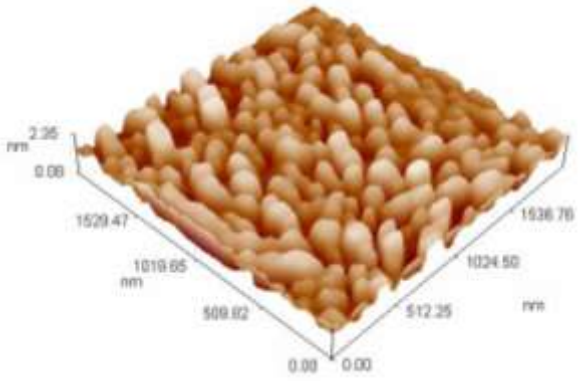

(x = 0.08)

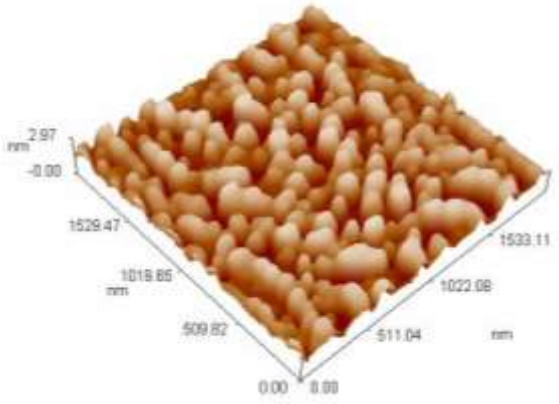

(x = 0.10)

Figure 3: The AFM images of $Ni_{(1-x)}Zn_{(x)}Fe_2O_4$ thin films

Table 3: Surface roughness, root mean square (RMS) and grain size of $Ni_{(1-X)}Zn_{(X)}Fe_2O_4$ thin films

$Ni_{(1-x)}Zn_{(x)}Fe_2O_4$			
x	**Surface roughness (nm)**	**RMS (nm)**	**Grain size (nm)**
0	0.481	0.559	102.58
0.02	0.473	0.544	95.11
0.04	0.358	0.419	93.21
0.06	0.319	0.370	92.63
0.08	0.273	0.312	91.49
0.10	0.248	0.283	82.61

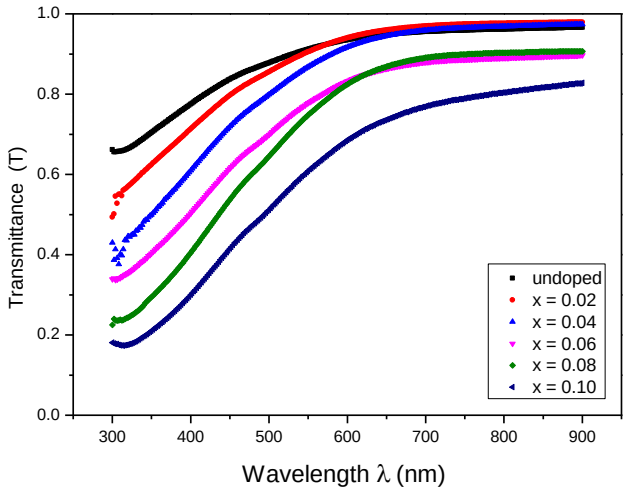

Figure 4: Transmittance (T) versus wavelength (λ) of $Ni_{(1-x)}Zn_{(x)}Fe_2O_4$ thin films

Figure 5 shows the absorbance (A) spectra of Nickel-Zinc Ferrite thin films. It can be noticed that the absorbance decreases as the concentration of Zinc increases and this can be attributed to the localized conductivity levels introduced by Zn^{2+} cations. The absorbance increases at short wavelengths (high energies) corresponding to the energy gap of the films, (when the incident photon has an energy equal or more than the energy gap value). This is due to the interaction of the material electrons with the incident photons which have enough energy for the occurrence of electron transitions.

The absorption coefficient can be estimated from the absorbance using the formula[28]:

$$\alpha = (2.303 * A) / t \qquad [2]$$

Where (A) is the absorbance, (t) is the thickness and (α) is the absorption coefficient. It have been noticed that all films have high absorption coefficient in the visible range of the spectrum, and this could be seen in **Figure 6**. It can be observed also that the absorption coefficient increases with increasing photon energy due to decrease in transmittance. The absorption coefficient increased with Zn concentration and

this may be due to the increase in lattice stress caused by the larger ionic radius of Zn ions[29]. The optical energy band gap (E_g) is given by the relation[30]:

$$\mathbf{A(h\nu - E_g)^r = h\nu\alpha} \qquad [3]$$

The optical energy gap can be calculated for all films by using Tauc's plot. **Figure 7** shows the plot of $(\alpha h\nu)^2$ vs. hν. The energy gap (E_g) was determined by assuming allowed direct transition between valance and conduction bands where r takes a value of ½ in equation (3). The energy gap values depend in general on the films crystal structure, the arrangement and distribution of atoms in the crystal lattice.

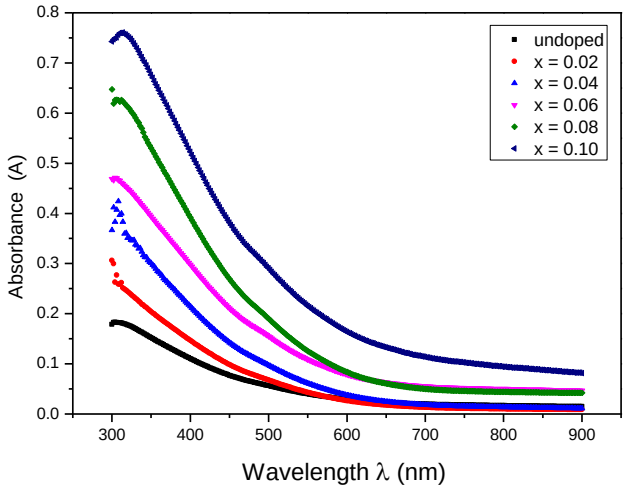

Figure 5: Absorbance (A) versus wavelength (λ) of $Ni_{(1-X)}Zn_{(x)}Fe_2O_4$ thin films

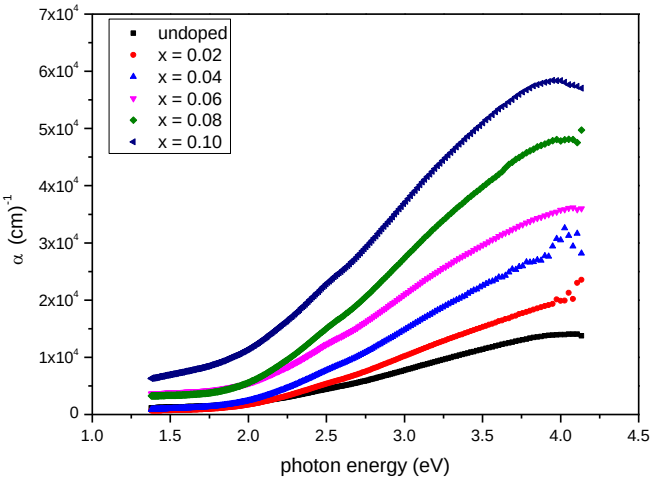

Figure 6: Absorption coefficient versus photon energy of $Ni_{(1-x)}Zn_{(x)}Fe_2O_4$ thin films

Plotting a graph between $(\alpha h\nu)^2$ and (hν) in eV, a straight line is obtained. The extrapolation of this straight line to $(\alpha h\nu)^2 = 0$ gives the value of the direct band gap of the material, and this is shown in **Figure 7**.

The allowed direct band gap values range between 2.96 eV and 2.85 eV for the prepared Samples.

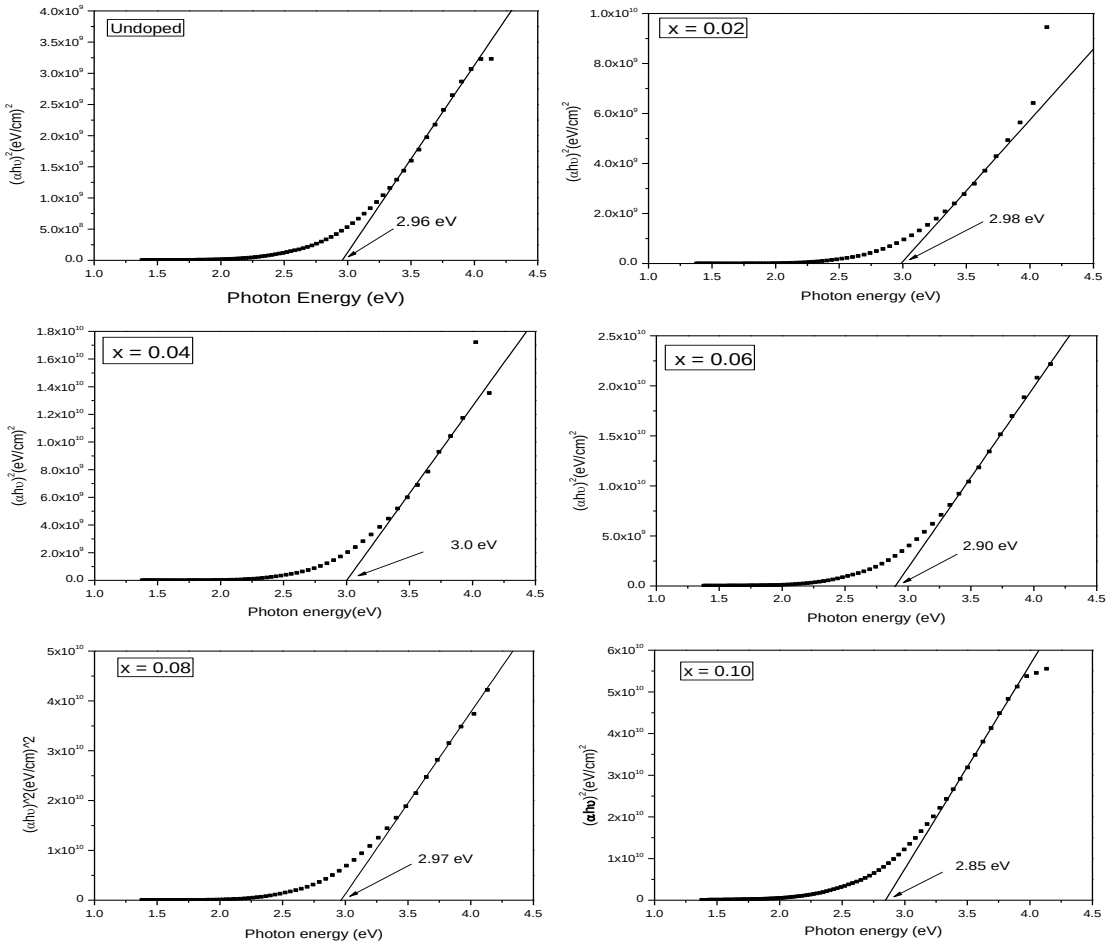

Figure 7: The relation between $(\alpha h\upsilon)^2$ and $(h\upsilon)$ for $Ni_{(x-1)}Zn_{(x)}Fe_2O_4$ thin films

The refractive index (n) for all films was determined using the relation[31]:

$$\mathbf{n} = \left[\left(\frac{1+R}{1-R}\right)^2 - \left(k_o^2 + 1\right)\right]^{1/2} + \frac{1+R}{1-R} \qquad [4]$$

The relation between refractive index and wavelength for spectrum range (300 – 900) nm of Nickel- Zinc Ferrite thin films is shown in **figure 8**.

The behavior of all figures reflects the typical dispersion relation in higher wavelength. In order to investigate the dispersion behavior of the prepared thin films, two terms of Cauchy's equation was applied to the n- λ data and the static refractive index (n_o) was calculated for all the prepared samples. Cauchy's equation is given by[32]:

$$n = a + \frac{b}{\lambda^2} \qquad [5]$$

The correlation coefficient (R^2) of the fitted dispersion relation was in the range of (0.81 - 0.98). The static refractive index (n_o) was in the range of (1.12- 1.19).

Extinction coefficient (K_o) of Nickel-Zinc Ferrite Oxide thin films was determined using the relation[31]:

$$K_o = (\alpha \lambda)/(4\pi) \quad [6]$$

Figure 9 shows the extinction coefficient as a function of wavelength of Nickel-Zinc Ferrite thin films. The extinction coefficient (K_o) increases at short wavelengths and after that the values of (K_o) decrease up to wavelength of ~ 600 nm and beyond this wavelength the values remain almost constant. The rise and fall in the value of (K_0) is directly related to the absorption of light. The lower value of (K_o) in the wavelength range (600–900) nm implies that these films absorb light in this region very easily. It can be noticed also that the extinction coefficient (K_o) increases with increasing the zinc concentration.

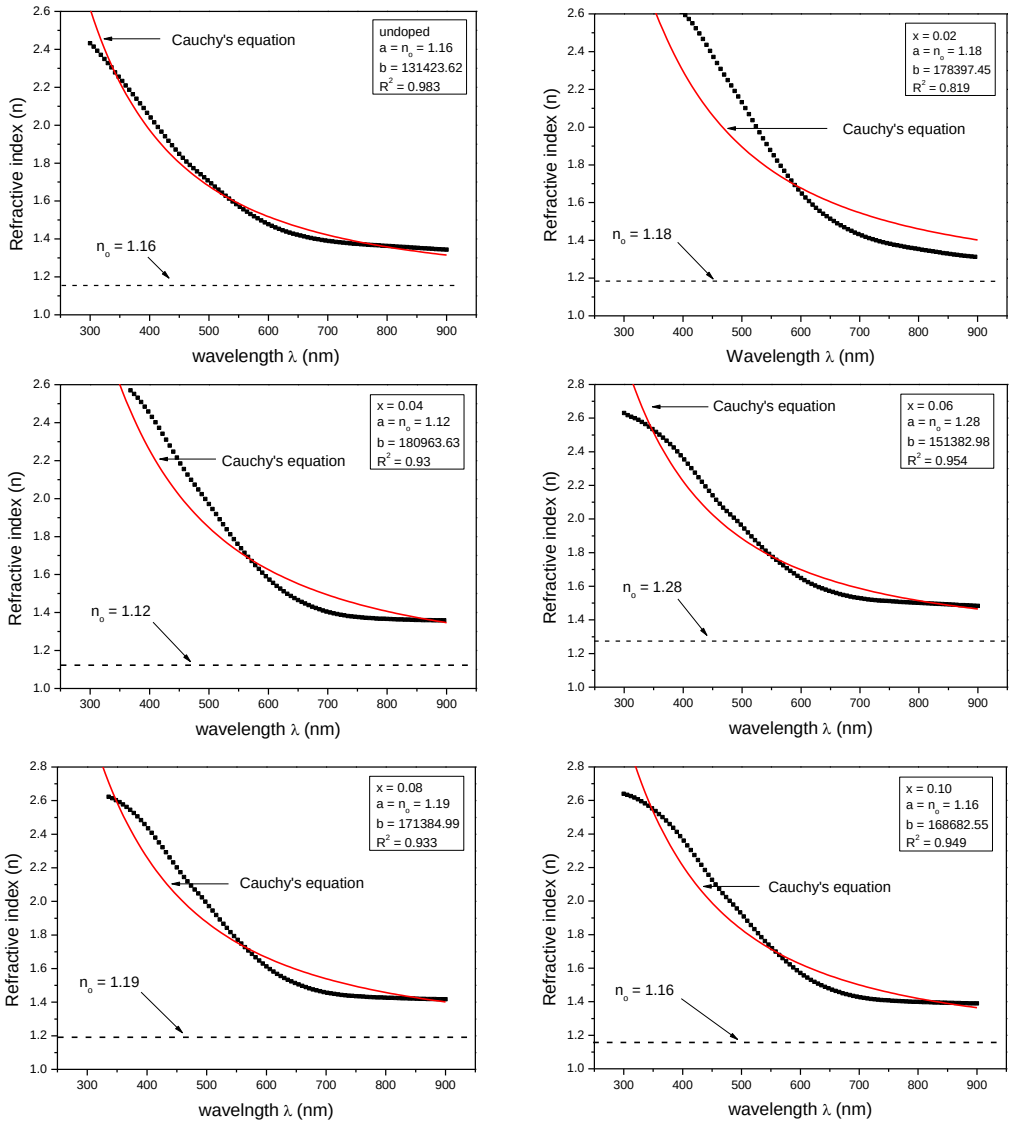

Figure 8: Refractive index as a function of wavelength of $Ni_{(1-x)}Zn_{(x)}Fe_2O_4$ thin films
The red line shows the Cauchy's equation fitting

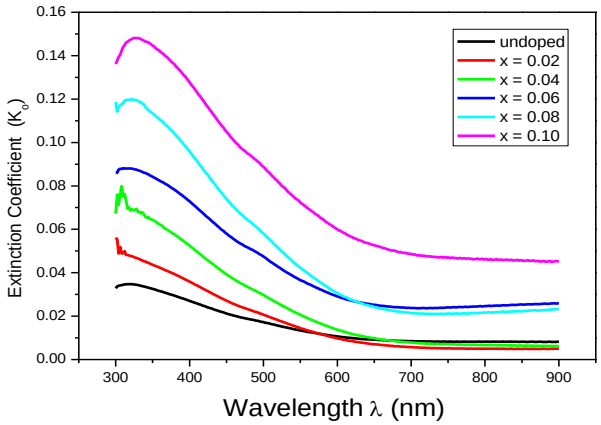

Figure 9: Extinction coefficient as a function of wavelength of $Ni_{(1-x)}Zn_{(x)}Fe_2O_4$ thin films

The real part (ε_1) and imaginary part (ε_2) of the dielectric constant can be calculated using the following equations[31]:

$$\varepsilon_1 = n_o^2 - k_o^2 \quad [7]$$

$$\varepsilon_2 = 2\, n_o\, k_o \quad [8]$$

The real part of dielectric constant (ε_1) is the normal dielectric constant and the imaginary part of the dielectric constant (ε_2) represents the absorption associated with free carriers. The real and imaginary parts of dielectric constant of Nicke-Zinc ferrite thin films as a function of photon energy are shown in **figure 10**. It can be seen that both the real and imaginary parts of the dielectric constant increase as photon energy increases in the visible region of the spectrum and after that the value of the real and imaginary parts decrease at higher energies.

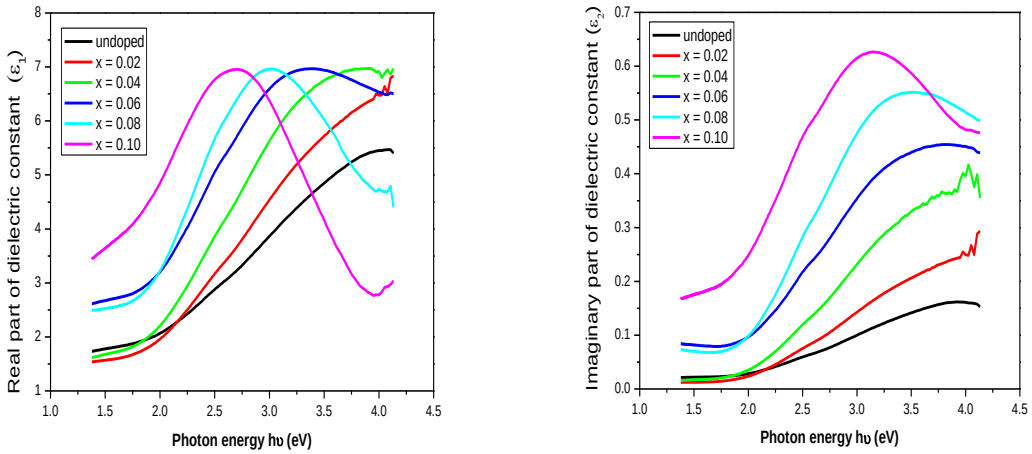

Figure 10: The real and imaginary parts of dielectric constant of $Ni_{(1-x)}Zn_{(x)}Fe_2O_4$ thin films as a function of photon energy

CONCLUSIONS

In this study Nickel-Zinc Ferrite ($Ni_{(1-x)}Zn_xFe_2O_4$) thin films, where (x = 0, 0.02, 0.04, 0.06, 0.08 and 0.10) were successfully deposited on glass substrate at (400 ± 10) ^oC by chemical spray pyrolysis technique. The XRD results showed that all films are polycrystalline in nature with cubic structure and the preferred orientation was along the (311) plane for all films. The crystallite size calculated by Scherrer's formula was found to be 14.18 nm for the undoped sample and decreases up to 3.94 nm for the sample with x = 0.10. It is observed also that lattice constant of Ni–Zn ferrite thin films increases with growing concentration of Zn^{2+}, and this may be attributed to the smaller Ni^{2+} cations of smaller ionic radii (0.74 Å) being replaced by larger Zn^{2+} cations of larger ionic radii (0.84 Å). Moreover, the addition of Zn^{2+} ions causes the migration of Fe^{3+} ions from tetrahedral sites to octahedral sites. The Zn^{2+} ions being larger than Fe^{3+} ions expand the tetrahedral sites leading to an increase in the lattice parameter. AFM results showed homogenous and smooth Nickel-Zinc Ferrite thin films. The AFM images show a uniform island-like topography and some structure of clusters, due to crystallites coalescence, could be clearly observed. The size of grains in clusters of $Ni_{(1-x)}Zn_{(x)}Fe_2O_4$ thin films are in the range of several tens of nanometers, which is one order of magnitude higher than the crystallite size calculated from XRD patterns. It is noticed that the absorbance of the prepared films decreases as the concentration of Zinc increases and this could be attributed to the localized conductivity levels introduced by Zn^{2+} cations. Due to the high values of absorption coefficient it is concluded that all films have direct band gap and its values range between 2.96 eV and 2.85 eV. Other optical parameters such as refractive index and dielectric constant are also affected by the zinc concentration.

REFERENCES

1. P. Tailhades, L. Bouet, L. Presmanes and A. Rousset, Thin-Film and fine powders of ferrites-materials for magneto optical recording media. J. Phys. 1997, 7(C1), 691-694
2. A. B. Gadkari, T. J. Shinde and P. N. Vasambekar, Ferrite gas sensors. IEEE Sens. J. 2011, 11, 849-861
3. K. S. Lin, A. K. Adhikari, Z. Y. Tsai, Y. P. Chen, T. T. Chien and H. B. Tsai, Synthesis and characterization of nickel ferrite nanocatalysts for CO_2 decomposition. Catal. Today 2011, 174, 88-96
4. E. Casbeer, V. K. Sharma and X. Z. Li, Synthesis and photocatalytic activity of ferrites under visible light: a review. Separation and Purification Technology, 2012, 87, 1–14
5. M. Sugimoto, The past, present and future of ferrites. J. Am. Ceram. Soc. 1999, 82, 269-280
6. R. Valenzuela, Novel Applications of Ferrites. Phys. Res. Int. 2012, 2012, 591839
7. Y. Liu, Y. Li, H. Zhang, D. Chen and C. Mu, Structural and magnetic properties of NiZn–ferrite thin films prepared by radio frequency magnetron sputtering. J. Appl. Phys. 2011, 109, 07A511
8. E. V. Rebrov, P. Gao, T. M. Verhoeven, J. C. Schouten and R. Kleismit, Structural and magnetic properties of sol-gel $Co_{2x}Ni_{0.5-x}$ $Zn_{0.5-x}Fe_2O_4$ thin films. J. Magn. Magn. Mater. 2011, 323, 723-729

9. M. Bohra, S. Prasad, N. Venkataramani, N. Kumar, S. C. Sahoo and R. Krishnan, Narrow Ferromagnetic Resonance Line width Polycrystalline Zn-Ferrite Thin Films. IEEE Trans. Magn. 2011, 47, 345-348.
10. P. A. Lane, P. J. Wright, M. J. Crosbie, A. D. Pitt, C. L. Reeves, B. Cockayne, A. C. Jones and T. J. Leedham, Liquid injection metal organic chemical vapour deposition of nickel zinc ferrite thin films. J. Cryst. Growth 1998, 192, 423-429**.**
11. T. H. Hai, H. T. B. Van, T. C. Phong and M. Abe, Spinel ferrite thin-film synthesis by spin-spray ferrite plating. Physica B, 2003, 327, 194-197
12. F. Liua, C. Yang, T. Ren, A. Z. Wang, J. Yu and L. Liu, NiCuZn ferrite thin films grown by a sol–gel method and rapid thermal annealing. J. Magn. Magn. Mater. 2007, 309, 75-79
13. A. Takayama, M. Okuya and S. Kaneko,Spray pyrolysis deposition of Ni Zn ferrite thin films. Solid State Ionics 2004, 172 , 257-260
14. Z. Wu, M. Okuya and S. Kaneko, Fluorine doped tin oxide film with high haze and transmittance prepared for dye-sensitized solar cells. Thin Solid Films 2001, 385, 109-114
15. L. X. Phua, F. Xu, Y. G. Ma and C. K. Ong, Structure and magnetic characterizations of cobalt ferrite films prepared by spray pyrolysis. Thin Solid Films 2009, 517(2), 5858–5861
16. D. Perednis and L. J. Gauckler, Spray pyrolysis of $La_{0.6}Sr_{0.4}Co_{0.2}Fe_{0.8}O_{3-\delta}$ thin film cathodes. J. Electroceram. 2005, 14, 103-111
17. M. Langlet, M. Labeau, B. Bochu and J. C. Joubert, Preparation of thin films in the system γFe_2O_3-Fe_3O_4 for recording media by spray pyrolysis of organometallic solutions using an ultrasonic pump. IEEE Trans. Magn. 1986, 22(3), 151-156
18. C. Barret and T. B. Massalki, Structure of Metals. 1980, Pergamon, Oxford
19. A. T. Raghavender, N. H. Hong, E. Chikoidze, Y. Dumont and M. Kurisu, Effect of zinc doping on the structural and magnetic properties of nickel ferrite thin films fabricated by pulsed laser deposition technique. J. Magn. Magn. Mater. 2015, 378, 358–361
20. J. Smith and H. P. J. Wijn, Ferrites 1959, John Wiley and Sons, New York
21. M. Sorescua, L. Diamandescu, R. Swaminathan, M. E. McHenry and M. Feder, Structural and magnetic properties of NiZn and Zn ferrite thin films obtained by laser ablation deposition. J. Appl. Phys. 2005, 97, 10G105
22. F. Shahbaz Tehrani, V. Daadmehr , A. T. Rezakhani , R. Hosseini Akbarnejad and S. Gholipour, Structural, magnetic, and optical properties of zinc- and copper- substituted nickel ferrite nanocrystals. Magnet and Superconducting Lab. 2009, 19938, Sharif University of Technology, Tehran, Iran
23. A. Y. Lipare, P. N. Vasambekar and A. S. Vainganka, X-ray, IR and dc electrical resistivity study of $CaCl_2$-doped zinc–copper ferrite system. Phys. Status Solidi 2003, 196(2), 372–378
24. S. M. Chavana, M. K. Babrekarc, S. S. Moreb and K. M. Jadhavc, Structural and optical properties of nanocrystalline Ni–Zn ferrite thin films. J. Alloy Compd. 2010, 507, 21–25
25. A. Takayama, M. Okuya and S. Kaneko, Spray pyrolysis deposition of NiZn ferrite thin films. Solid State Ionics 2004, 172, 257–260

26. J. I. Pankove, Optical Process in Semiconductors. 1971, Dover Publishing Inc., New York
27. R. E. van de Leest, F. Roozeboom, Nickel–zinc ferrite films by rapid thermal processing of sol–gel precursors. Applied Surface Science 2002, 187(1–2), 68–74
28. N. F. Al. Shammary, Optical characteristics of NiO thin film on glass formed by chemical spray pyrolysis. Journal of Kufa-Physics 2010, 2(1), 22-27
29. M. Ohring, The materials science of thin films 1992, Academic press, New York
30. K. L. Chopra, Thin film phenomena 1969, McGraw-Hill, USA
31. C. Hamaguchi, Basic Semiconductor physics 2001, Springer-Verlag, Berlin Heidelberg
32. N. A. Bakr, A. M. Funde, V. S. Waman, M. M. Kamble, R. R. Hawaldar, D. P. Amalnerkar, S. W. Gosavi, and S. R. Jadkar, Determination of the optical parameters of a-Si: H thin films deposited by hot wire–chemical vapour deposition technique using transmission spectrum only. Pramana 2011, 76(3), 519-531

*** Corresponding author: *Nabeel A. Bakr***

Department of Physics, College of Science, University of Diyala, Diyala, IRAQ